JOURNAL OF MATERIALS SCIENCE 12 (1977) 718–734

The thermal expansion of carbon fibre-reinforced plastics

Part 1 *The influence of fibre type and orientation*

K. F. ROGERS, L. N. PHILLIPS, D. M. KINGSTON-LEE
Materials Department, Royal Aircraft Establishment, Farnborough, UK

B. YATES, M. J. OVERY*, J. P. SARGENT, B. A. McCALLA
Department of Pure and Applied Physics, University of Salford, UK

Interferometric measurements of the linear thermal expansion coefficients between approximately 90 and 400 K of a series of unidirectional and bidirectional specimens of epoxy resin ERLA 4617/mPDA reinforced with Courtaulds HTS and HMS carbon fibres are reported for three mutually perpendicular directions. The room temperature results have been employed, in association with related data, to confirm that the main features of the dependence of the linear thermal expansion coefficients of these composites upon the thermal and elastic properties of the constituents and the orientations of the fibres within the matrices conform with expectations based upon current models of the thermal expansion and elastic behaviour of composite solids. At higher temperatures the results clearly show marked changes in the temperature dependence of the dimensional behaviour which result from the relaxation accompanying the softening of the resin.

1. Introduction

The advantages of the high stiffness and strength to weight ratios offered by carbon fibre–epoxy resin composites are well known. In order to achieve particular elastic properties in preferred directions, continuous carbon fibres are usually employed in structures having essentially two-dimensional characteristics. For convenience of construction, the fibres in the form of multifilament tows are laid parallel and impregnated with the matrix resin to form an uncured unidirectional lamina or ply. The final structure is then produced by stacking the plies in an appropriate sequence and curing under heat and pressure to form a rigid laminate which possesses the directional characteristics required.

Correlations of the elastic constants and the coefficients of linear thermal expansion with the ply stacking sequence form the subject of a number of analytical calculations. A correct understanding of these relationships is clearly of enormous potential value in the science and technology of this class of composites, since it opens up the possibility of applying known thermoelastic properties of the constituents to the design of structures having required directional properties.

The experimental data upon which observation and prediction have been compared in the composites field are comparatively limited. This is particularly true of the thermal expansion of carbon fibre-reinforced plastics, where data which do exist are usually restricted to room temperature. Because practical applications of these materials operate over a wide range of temperature, the linear thermal expansion coefficients of a series of unidirectional and cross-plied carbon fibre-reinforced epoxy resin specimens were investigated systematically between approximately 80 K and the temperature region above 400 K in which resin softening prevented further meaningful measure-

* Present address: North Salford High School, Salford, UK

ments; with the object of (i) providing information of direct technological value and (ii) exploring the extent to which current ideas concerning thermoelastic effects in two-phase composites could account for the observed behaviour.

2. The specimens

2.1. Constituent materials

Matrix type, fibre type, fibre volume fraction and inter-ply angle provide a wide variety of combinations, so that selection was necessary before a measurement programme could commence. For the programme reported here one epoxy resin matrix, two types of carbon fibre and one nominal fibre content by volume (50%) were chosen. The resin was ERLA 4617, batch B14, obtained from Bakelite Xylonite Ltd, and hardened with metaphenylene diamine obtained from Anchor Chemicals Ltd. The type I fibres were Courtaulds HMS batch QM 218/622W, and the type II fibres were Courtaulds HTS batch PT 112/21Z, both made from polyacrylonitrile precursor.

According to the suppliers, ERLA 4617 is a copolymer of di(epoxy cyclopentyl) ether and ethylene glycol, catalysed with benzyl dimethylamine. Prior to use, it was pre-polymerized with the stoichiometric quantity of metaphenylene diamine in acetone solution in accordance with the manufacturer's recommended schedule, giving a prepolymer solution containing 50% by weight of resin.

The test bars (so called for convenience although some were flat laminates) were produced as described below. The greater part of the current programme formed an extension of work begun earlier [1], but for completeness the descriptions of the earlier specimens are included.

2.2. Pure resin test bar

To prepare the cast resin bar pre-polymer prepared as above but without the addition of acetone was poured into a 75 mm × 13 mm bar mould and cured for $2\frac{1}{2}$ h at 100° C, 2 h at 170° C and 6 h at 200° C. A specimen for void determination was then cut from a position at the centre of the bar adjacent to that from which the thermal expansion specimens were to be cut. This specimen was scanned ultrasonically and the constant attenuation observed was interpreted as indicating that if voids were present they were uniformly distributed. Smaller specimens cut from the test bar were potted and polished. Examination of these under the microscope revealed them to be void-free and glass-clear.

2.3. Unidirectional bars

To prepare the unidirectional carbon fibre reinforced bars the fibre tows, each consisting of 10^4 parallel fibres, were set up twist-free on a frame and maintained under light tension by rubber bands, in order to preserve a high degree of parallel fibre alignment. The pre-polymer solution was added to the tows, which were then air-dried overnight and precured for $2\frac{1}{2}$ h at 100° C still under tension. The tows were then removed from the

TABLE I The specimens

Bar number	Specimen designation	Fibre type	Angle between fibre directions (deg)	Direction of thermal expansion measurements	Fibre volume (%)	Void content (%)
1	1	No fibres			0.0	0.0
2	2	HTS	0	Parallel to fibres	49.4	1.9
2	3	HTS	0	Perpendicular to fibres	49.4	1.9
2	4	HTS	0	45° to fibres	49.4	1.9
3	5	HTS (pre-preg)	90	Parallel to one set of fibres	50.0	0.0
3	6	HTS (pre-preg)	90	Bisecting angle between fibres	50.0	0.0
3	7	HTS (pre-preg)	90	Perpendicular to plane of laminate	50.0	0.0
4	8	HTS	63	Bisecting acute angle	52.9	4.2
4	9	HTS	63	Bisecting obtuse angle	52.9	4.2
5	10	HMS	0	Parallel to fibres	50.4	1.6
5	11	HMS	0	Perpendicular to fibres	50.4	1.6
6	12	HMS	90	Parallel to one set of fibres	52.0	0.0
6	13	HMS	90	Bisecting angle between fibres	52.0	0.0
6	14	HMS	90	Perpendicular to plane of laminate	52.0	0.0
7	15	HMS	66	Bisecting acute angle	52.6	0.2
7	16	HMS	66	Bisecting obtuse angle	52.6	0.2
7	17	HMS	66	Perpendicular to plane of laminate	52.6	0.2

frame, cut to length, aligned carefully in an open-ended 150 mm x 12.5 mm x 12.5 mm bar mould, cured under closing pressure for 2 h at 170° C and postcured for 6 h at 200° C.

2.4. Bidirectional bars

To prepare the cross-plied and angle-plied laminates the tows were set up twist-free on the frame and impregnated and pre-cured as before, but the precure was reduced to 2 h at 100° C. After precure, each tow was flattened into a 3.5 mm wide tape by hand roller to give a ply thickness of 0.25 mm in the finished laminate. The flattened tows were laid up in a 75 mm x 75 mm x 6.35 mm flat mould, 13 plies in one direction alternating with 12 plies in the other direction, the angle between the two directions being as in Table I. The laminates were press-moulded and post-cured as before. The calculated fibre volumes and void contents are given in Table I. The bars were constructed from single tows because of the high degree of control over fibre alignment that this method of assembly permits. For reasons explained later a further test bar was prepared by a different method.

2.5. Bidirectional bar made from commercial pre-preg

This bar (bar 3 of Table I) was prepared from commercially pre-impregnated sheets of Courtaulds HTS fibre and ERLA 4617/mPDA resin. The prepreg was laid up in the mould without further precure, 25 plies at 0° alternating with 25 plies at 90°, to give a finished laminate thickness of 12.7 mm. The laminate was press-moulded and post-cured as before.

2.6. Specimen preparation

Following the procedure described earlier [1], pieces approximately 13 mm long were rejected from each end of the bars, and sets of three specimens 10 to 13 mm long were cut from the remaining portion using a tungsten wire saw loaded with carborundum powder. Although rather slow, this procedure ensured that the temperature of the bars did not rise significantly during specimen preparation. The cut surfaces were finished on a surface grinder and the ends of the specimens were ground by hand so as to be slightly dome-shaped. Each specimen had typically a square cross-section of side 5 to 6 mm, and full use was made of the original side faces of the bars to ensure that the specimens had the correct orientation when standing upright in the interferometer employed for the thermal expansion measurements.

To ensure that the specimens prepared from the bar 12.7 mm thick produced from commercial prepreg had a geometry comparable to that of the specimens prepared from tows, portions of the bar were ground to the thickness of a 13 ply/12 ply laminate (6.35 mm) before specimens were cut from them.

3. Experimental details

3.1. The apparatus

Each set of three specimens was employed in turn to provide the separation of a pair of optical flats comprising a Fizeau interferometric arrangement, the specimen support being of the type described earlier [1]. The apparatus employed below room temperature was based upon that described originally by James and Yates [2], but having improved thermometry, better temperature control and easier access to the specimens. The apparatus used above room temperature was described originally by Pojur and Yates [3]. The versatility of this apparatus had been improved by the incorporation of an additional optical flat between the specimens and the prism, and the limits between which specimen temperatures could be held constant had been reduced by re-siting the sensing thermocouple of the temperature controller. Full details of the latest forms of both sets of apparatus have been described by Overy [4].

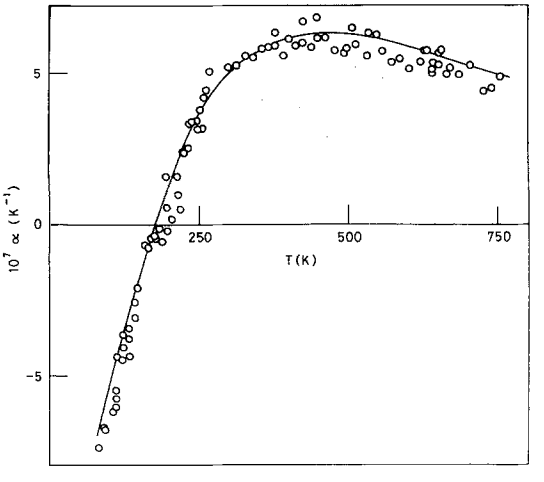

Figure 1 The linear thermal expansion coefficient α of fused silica (SRM 739 from the National Bureau of Standards): o present primary data; ——— smoothed NBS data [5].

TABLE II Smoothed values of the linear thermal expansion coefficients α of the specimens described in Table I

T (K)	α (K^{-1}) for the specimens numbered below																
	1 $\times 10^{-5}$	2 $\times 10^{-7}$	3 $\times 10^{-5}$	4 $\times 10^{-5}$	5 $\times 10^{-6}$	6 $\times 10^{-6}$	7 $\times 10^{-5}$	8 $\times 10^{-5}$	9 $\times 10^{-5}$	10 $\times 10^{-7}$	11 $\times 10^{-5}$	12 $\times 10^{-6}$	13 $\times 10^{-6}$	14 $\times 10^{-5}$	15 $\times 10^{-5}$	16 $\times 10^{-5}$	17 $\times 10^{-5}$
90	2.31	3.3	1.66	(0.83)	2.78		2.24	−0.13	0.72		1.90	1.43	1.20	2.65	−0.17	0.84	2.61
100	2.43	3.0	1.79	0.90	2.84	(3.06)	2.38	−0.14	0.78	−2.0	2.00	1.44	1.25	2.80	−0.20	0.87	2.75
120	2.68	2.5	2.02	1.01	2.95	3.20	2.66	−0.17	0.87	−2.8	2.19	1.45	1.33	3.10	−0.24	0.93	3.01
140	2.93	1.9	2.21	1.11	3.07	3.32	2.91	−0.19	0.94	−3.6	2.36	1.48	1.39	3.33	−0.26	1.00	3.29
160	3.16	1.3	2.41	1.21	3.21	3.45	3.19	−0.21	1.01	−4.7	2.54	1.52	1.42	3.58	−0.28	1.06	3.52
180	3.38	0.6	2.56	1.29	3.35	3.58	3.42	−0.22	1.08	−5.6	2.70	1.57	1.46	3.80	−0.30	1.12	3.78
200	3.61	0.0	2.70	1.37	3.51	3.71	3.68	−0.24	1.13	−5.7	2.84	1.64	1.50	4.00	−0.31	1.18	4.00
220	3.83	−0.4	2.83	1.43	3.67	3.86	3.89	−0.24	1.17	−5.2	2.99	1.72	1.56	4.20	−0.31	1.24	4.20
240	4.00	−0.8	2.91	1.48	3.86	4.00	4.09	−0.25	1.21	−4.6	3.11	1.83	1.63	4.37	−0.32	1.30	4.40
260	4.18	−1.4	2.99	1.50	4.09	4.16	4.29	−0.26	1.21	−3.7	3.21	1.97	1.72	4.50	−0.34	1.36	4.57
280	4.32	−1.8	3.08	1.51	4.35	4.33	4.60	−0.26	1.24	−3.0	3.31	2.14	1.82	4.62	−0.37	1.42	4.73
300	4.50	−2.6	3.27	1.59	4.66	4.53	5.05	−0.27	1.34	−2.6	3.39	2.40	1.95	4.83	−0.42	1.49	4.95
320	4.78	−2.2	3.60	1.76	5.15	4.76	5.73	−0.30	1.50	−2.6	3.46	2.67	2.11	5.40	−0.50	1.64	5.46
340	5.33	0.2	4.11	2.07	5.55	5.02	6.83	−0.37	1.76	−2.8	3.64	2.75	2.30	6.40	−0.62	1.92	6.78
360	6.21	1.2	4.81	2.51	5.65	5.35	8.34	−0.48	2.15	−3.6	4.03	2.42	2.59	8.20	−0.82	2.56	9.60
380	7.37	0.2	5.86	3.19	5.55	5.80	10.4	−0.74	2.77	−4.6	4.75	1.60	3.10	12.5	−1.51		15.6
390	8.11	−0.8	6.70	3.70	5.42	6.11	11.8	−1.04	3.26	−5.2	5.34	0.54					20.8
400		−2.2		4.49	5.25	6.50	13.6	−1.46		−6.3	6.29						26.5
410		−4.2			4.98	6.98	16.1	−2.21		−7.3							
420		−6.6			4.61					−9.0							
430		−11.0			4.06					−11.0							
440					3.23					−14.7							
460					1.22												

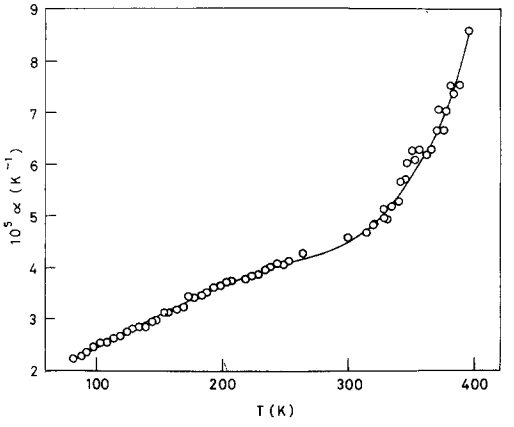

Figure 2 The linear thermal expansion coefficient α of specimens 1.

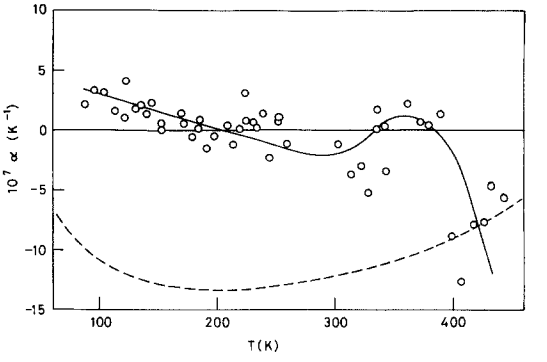

Figure 3 The linear thermal expansion coefficient α of specimens 2: ○ primary data; – – – – – smoothed results for pyrolytic graphite in a direction perpendicular to the *c*-crystallographic axis [8, 9].

3.2. Standardization of the apparatus

It became apparent at an early stage of the investigation that the linear thermal expansion coefficients to be measured would be very small, and it was deemed necessary to establish the capability of the apparatus by measuring the linear thermal expansion coefficient of a standard low expansion reference material and comparing the results with accepted values. Specimens of standard fused silica SRM 739 obtained from the US National Bureau of Standards were employed for this purpose; the results are compared in Fig. 1 with the smoothed data of Kirby and Hahn [5]. The two sets of results agree within experimental error.

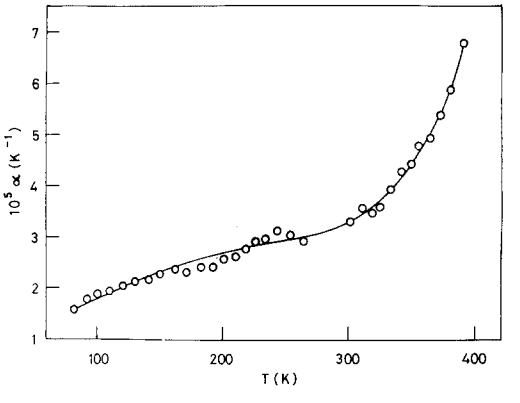

Figure 4 The linear thermal expansion coefficient α of specimens 3.

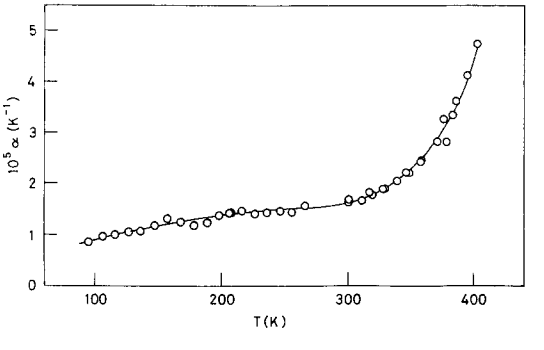

Figure 5 The linear thermal expansion coefficient α of specimens 4.

4. Results

4.1. Preliminary considerations

For convenience of analysis, the coefficients of linear thermal expansion of the carbon fibre composite bars are summarized in smoothed form in Table II. In order to highlight features which would not otherwise be apparent the primary data are displayed in graphical form in Figs. 2 to 18. The values given in Table II were taken from best lines drawn by eye through the data points of the figures.

The original set of six bars made by the individual tow alignment process included one made in HTS fibre, 13 plies at 0° alternated with 12 plies at 90°, analogous to bar 6. Measurements upon specimens cut from this bar with their axes bisecting the angle between the fibres were unexpectedly and substantially higher than those for other specimens cut from the same bar with their axes parallel to one set of fibres. It was thought that this difference in expansion might be an effect of the small size of the interferometric specimens, and therefore the much larger laminate, bar 3, was made up from commercial pre-preg. Specimens 100 mm x 12.7 mm x 12.7 mm were cut from this bar at 0° and at 45° to the principal fibre axis and were submitted to an independent laboratory for thermal expansion determination by dilatometer. The results obtained were insufficiently precise to

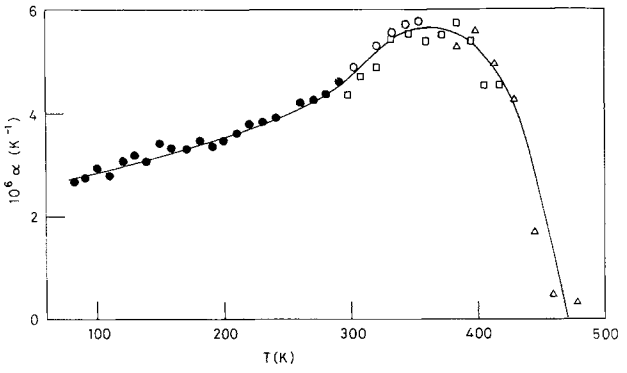

Figure 6 The linear thermal expansion coefficient α of specimens 5: • low temperature runs; ○ 1st, □ 2nd and △ 3rd high temperature runs.

be meaningful, and so the remainder of the bar was reduced to a 6.4 mm thick alternate 13 ply/12 ply laminate by grinding, as previously stated, and a set of small specimens at 0° and another set at 45° were cut from it for interferometric study. These are specimens 5 and 6 of Table 1. The anomalous difference in expansion did not appear in these specimens and was attributed to an abnormally high void content (5.5%) in the original bar. Because of this high void content the results for the original bar are not reported here.

Calculations indicated that the linear thermal expansion coefficients of specimens cut from the two fibre directions of a 13 layer/12 layer alternated 0°/90° cross-plied laminate should differ by about 10%. Subsequent measurements have revealed that this is no greater than the variation observed with the position within a bar. For consistency, however, specimens 5 and 12 were both cut so that the axis of measurement was parallel to the fibres in the 13 ply direction.

In a further subsidiary investigation, the possible effect of the single-tow hand lay-up of the unidirectional bars upon the expansion transverse to the fibre direction was examined. As the mould closes during the press-moulding process the circular cross-sections of the fibre tows are compressed into ellipses with their major axes transverse to the fibre direction and in the plane of the laminate, and their minor axes transverse to the fibre direction but normal to the plane of the laminate. It was thought that there might be a difference in fibre-resin distribution in these two transverse directions which might produce a difference in thermal expansion. To check this, two sets of specimens with axes perpendicular to the fibre direction were cut from bar 5. The first set had axes parallel to the plane of the laminate; the second set had axes normal to this plane. The

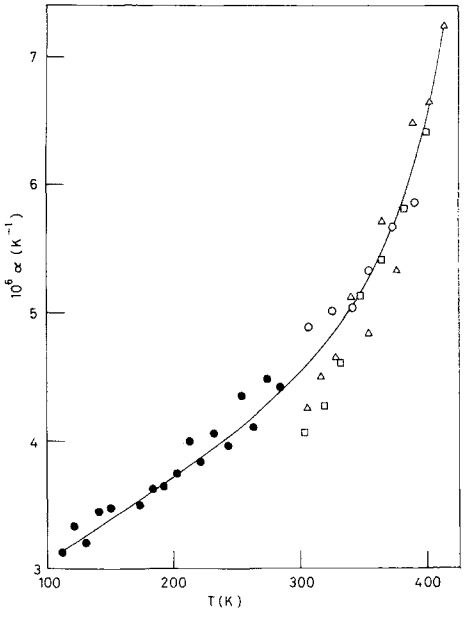

Figure 7 The linear thermal expansion coefficient α of specimens 6; • low temperature runs; ○ 1st, □ 2nd and △ 3rd high temperature runs.

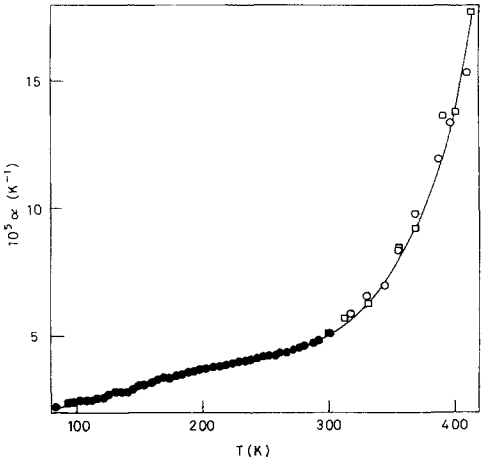

Figure 8 The linear thermal expansion coefficient α of specimens 7: • low temperature runs; ○ 1st and □ 2nd high temperature runs.

linear thermal expansion of each set was investigated between approximately 80 and 300 K. The results of the two investigations were indistinguishable, indicating the existence of a plane of isotropic expansion perpendicular to the fibre direction.

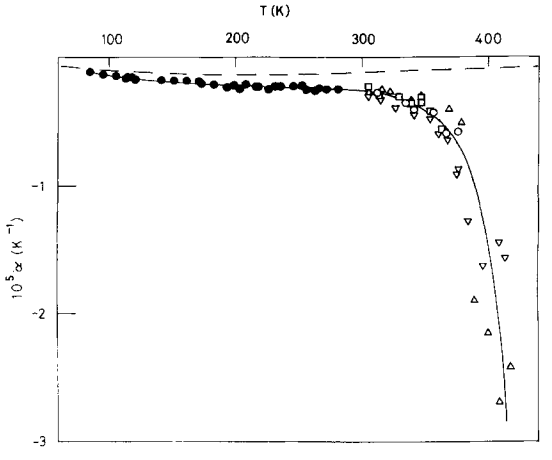

Figure 9 The linear thermal expansion coefficient α of specimens 8: • low temperature runs; ○ 1st, □ 2nd, △ 3rd and ▽ 4th high temperature runs; – – – – – smoothed results for pyrolytic graphite in a direction perpendicular to the *c*-crystallographic axis [8, 9].

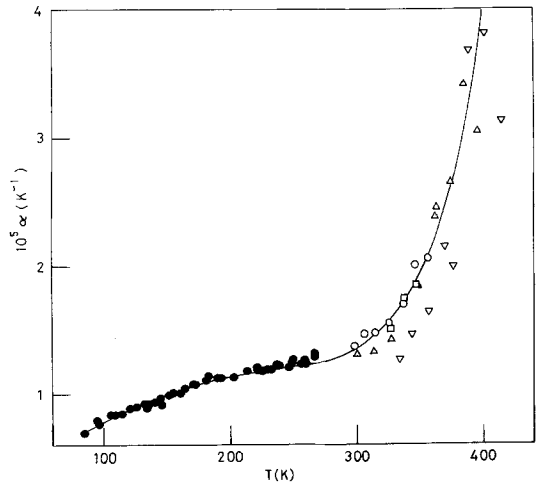

Figure 10 The linear thermal expansion coefficient α of specimens 9: • low temperature runs; ○ 1st, □ 2nd, △ 3rd and ▽ 4th high temperature runs.

It was desired to correlate the experimental results with theoretical models, but prior to attempting this it was necessary to examine the results for reproducibility. For this reason each part of each temperature region through which the specimens were cycled was almost invariably traversed at least twice. The results of the low temperature measurements, i.e. those conducted below room temperature were invariably reproducible. For the high temperature measurements, i.e. those conducted above room temperature, the behaviour was less simple. During the course of high temperature measurements upon specimens in which the expansion behaviour was dominated by the resin it became apparent that sets of results obtained during the rising portion of successive temperature cycles terminating at increasingly higher temperatures were sometimes successively lower in value than the preceding sets. Further investigation revealed that the occurrence of this effect was not affected by the sequence in which the specimens were taken through the low temperature and high temperature measurement cycles, the effect invariably occurring at high temperatures. It was further established that if the ends of the specimens were lightly ground after the manifestation of such a shift, the subsequent variation of the expansion coefficient reverted to its earlier values. Because of these observations the order of the high temperature runs was recorded for reference purposes. This type of behaviour has not been observed in earlier investigations employing the apparatus to investigate single-phase solids at temperatures well below their melting points, i.e. the effect was undoubtedly a characteristic of the specimens and not of the apparatus. Figs. 10 and 14 provide illustrations of this behaviour, the origin of which remains unknown. When the phenomenon did occur, the characteristic behaviour of the composite was taken to be that depicted by the results taken early in the sequence of measurements.

Finally it may be mentioned that the influence of the shapes of the non-rectangular ends of the

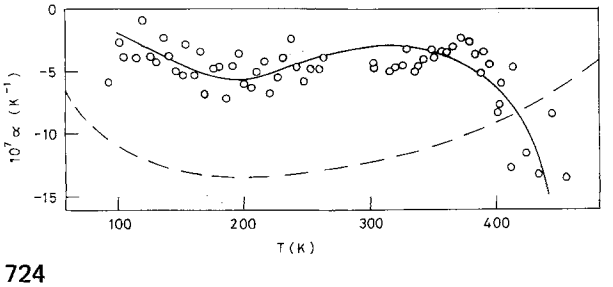

Figure 11 The linear thermal expansion coefficient α of specimens 10: ○ primary data; – – – – – smoothed results for pyrolytic graphite in a direction perpendicular to the *c*-crystallographic axis [8, 9].

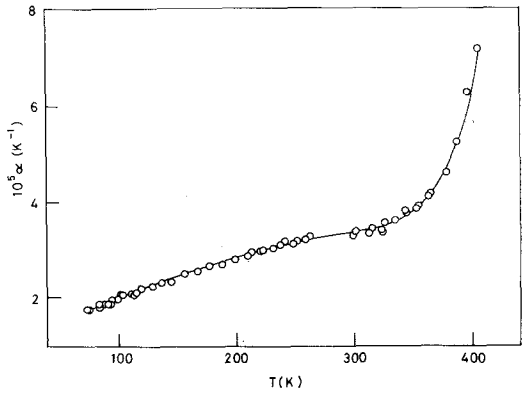

Figure 12 The linear thermal expansion coefficient α of specimens 11.

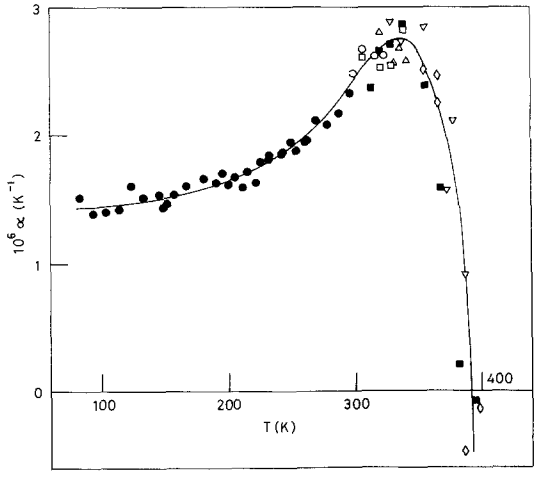

Figure 13 The linear thermal expansion coefficient α of specimens 12: • low temperature runs; ○ 1st, □ 2nd, △ 3rd, ▽ 4th, ◇ 5th and ■ 6th high temperature runs.

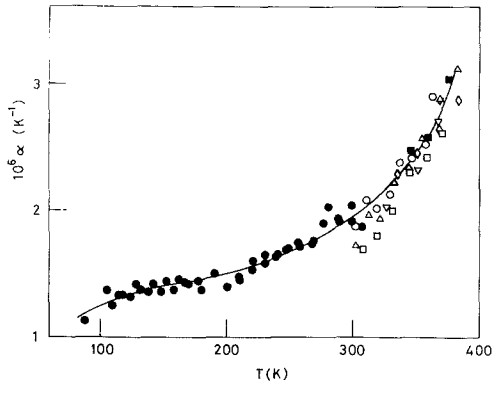

Figure 14 The linear thermal expansion coefficient α of specimens 13: • low temperature runs; ○ 1st, □ 2nd, △ 3rd, ▽ 4th, ◇ 5th and ■ 6th high temperature runs.

specimens upon the experimental results was investigated experimentally and theoretically. Both investigations indicated that such influence was negligible in comparison with other experimental uncertainties.

4.2. Comparison with related work

Although isolated determinations of the linear thermal expansion coefficients of carbon fibre-reinforced plastics have been reported in the literature, the variations afforded by resin type, fibre type, fibre volume fraction and specimen geometry are too extensive to permit useful direct comparisons with individual cases within the present investigation. Perhaps the most systematic experimental studies are those of Fahmy and Ragai [6, 7], who observed qualitative agreement between the measured and calculated directional thermal expansion characteristics of their unidirectional and bidirectional laminates. In general terms the present results confirm the findings of Fahmy and Ragai where the investigations overlap. The present results, however, are believed to be the first of their kind to display the temperature dependence of these characteristics systematically, and hence meaningful comparison with earlier work is not possible.

5. Discussion

5.1. Qualitative observations

5.1.1. Specimens 1

As may be seen from Fig. 2, the results for the pure resin displayed no unusual features at temperatures below the region 280 to 320 K. Within this range, however, the rate at which the slope was changing increased quite rapidly and finally measurements became impossible because of abrupt changes in the interference fringe pattern. Speculations as to the origin of the marked change in the variation between 280 and 320 K have been offered earlier [1].

5.1.2. Specimens 2 (HTS fibres) and 10 (HMS fibres)

The qualitative similarity of the thermal expansion behaviour in the fibre direction of the unidirectional specimens containing the two types of fibre is apparent from a comparison of Figs. 3 and 11. Results for pyrolytic graphite in the α–α plane of the crystallites [8, 9] are included in the two figures, from which it appears that the contraction

of the fibres in the direction of their length is dominating the behaviour at the lower temperatures. At temperatures where the thermal expansion of the resin is rising increasingly rapidly, however, the results for the composite proceed to rise, suggesting that an increasingly important part is being played by the resin in this region. At still higher temperatures, the composite expansion falls to increasingly negative values as the resin commences to soften and, apparently, allows the fibres to dominate the behaviour of the composite again. The similarity of the corresponding features in the two cases is consistent with this pattern of behaviour and, as is to be expected from the closer alignment of the basal planes of the crystallites with the fibre direction in the HMS fibre, the results of specimens 10 are numerically more negative than those for specimens 2. At high temperatures the thermal expansion of both sets of specimens is more negative than that of pyrolytic graphite in the α–α plane. This is particularly true of specimens 10, and it is reasonable to suppose that the fibres themselves must have even more negative thermal expansion coefficients in the direction of their lengths. The structure of the fibres is known to be complex [10–13]. For this reason the higher temperature dimensional changes may be caused by a combination of structural changes and changes in inter-atomic separation.

5.1.3. Specimens 3 (HTS fibres) and 11 (HMS fibres)

A comparison of Figs. 2, 4 and 12 reveals that the thermal expansions of the two sets of unidirectional specimens transverse to the fibre direction are very similar to one another, this essentially common expansion being somewhat lower than the corresponding results for the pure resin. Although the structure of the fibres is almost certainly more complex than that of pyrolytic graphite, the linear thermal expansion coefficients of pyrolytic graphite are frequently assumed for carbon fibres, in the absence of better approximations. On the basis of such an association of the *c*-axis expansion of pyrolytic graphite with the transverse direction of the fibres, the observed relative magnitudes of the thermal expansions of specimens 3 and 11 and the pure resin is to be expected. The similarity of the results for specimens 3 and 11 indicates the similarity of the transverse expansions of the HTS and HMS fibres.

5.1.4. Specimens 4 (HTS fibres)

It was shown earlier [1] how the results shown in Fig. 5 for this specimen at 45° to the fibre direction were consistent with the equation

$$\alpha_\theta^c = \alpha_1^c \cos^2\theta + \alpha_2^c \sin^2\theta$$

for the linear thermal expansion coefficient of a unidirectional composite in a direction inclined at and angle θ to the fibres, α_1^c, α_2^c and α_θ^c being the linear thermal expansion coefficients of the composite in directions parallel, perpendicular and at angle θ to the fibres respectively.

5.1.5. Specimens 5 (HTS fibres) and 12 (HMS fibres)

Figs. 6 and 13 show the distinctive character of the temperature variations of the linear thermal expansion coefficients of the two 90° cross-plied laminates in a direction parallel to one set of fibres. A temperature dependence intermediate between those of specimens 2 and 10 on the one hand and specimens 3 and 11 on the other is to be expected, as the relative influences of the resin and fibres vary with temperature. As the resin softens at the higher temperatures the dominating influence of the fibres becomes apparent in a manner resembling that seen in specimens 2 and 10. Consistent with the more complete alignment of the crystallites in the HMS fibres, corresponding features of temperature dependence occur at lower temperatures in specimens 12 than in specimens 5 and the expansion coefficients at these corresponding features are also lower.

5.1.6. Specimens 6 (HTS fibres) and 13 (HMS fibres)

Symmetry considerations lead one to expect the linear thermal expansion coefficient in the plane of a 0°/90° balanced and equally cross-plied laminate to be independent of direction. For the two cases covered by this investigation a comparison of the results for the direction parallel to one set of fibres and for a direction bisecting the inter-ply angle of 90° shows that before resin softening effects become serious this is indeed the case. When comparing the results of Fig. 6 with those in Fig. 7, and those in Fig. 13 with those in Fig. 14, a reasonable allowance for the unavoidable imperfections found in real specimens which cause departures from the behaviour of hypothetically ideal specimens must be made. At higher tem-

peratures, however, the dominating influence of the fibres again appears, this time in the increasingly rapid rise of the linear thermal expansion coefficient with temperature in specimens 6 and 13.

5.1.7. Specimens 8 (HTS fibres) and 15 (HMS fibres)

One of the conclusions emerging from the work of Halpin and Pagano [14] was that marked negative expansional strains were to be expected over a range of fibre orientations in physical systems resembling the cross-plied laminates of the present investigation. These authors produced experimental evidence for the validity of their conclusions using an elastomeric matrix reinforced with nylon textile cords, swelling of the matrix being induced by immersion in benzene. Figs. 9 and 16 show the thermal expansion results obtained for specimens

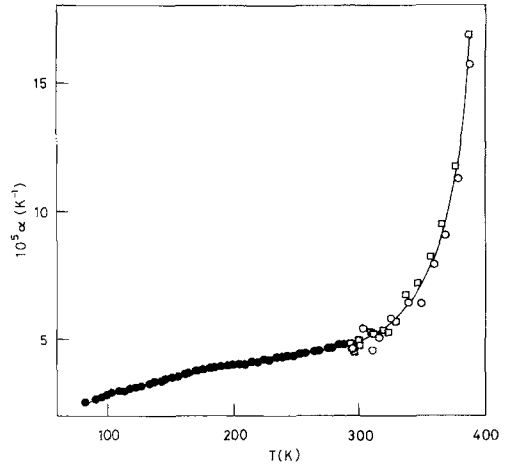

Figure 15 The linear thermal expansion coefficient α of specimens 14: • low temperature runs; ○ 1st and □ 2nd high temperature runs.

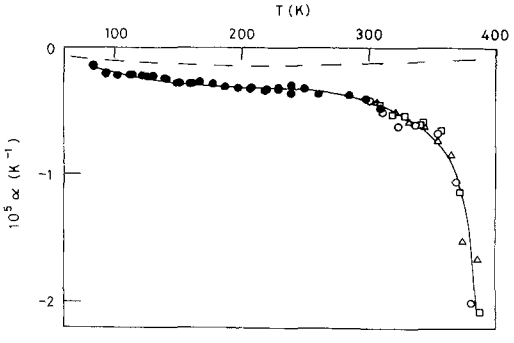

Figure 16 The linear thermal expansion coefficient α of specimens 15: • low temperature runs; ○ 1st, □ 2nd and △ 3rd high temperature runs; – – – – – smoothed results for pyrolytic graphite in a direction perpendicular to the *c*-crystallographic axis [8, 9].

8 and 15, in which the direction of measurement bisected the acute inter-ply angle of the angle-plied laminates. The temperature variations of the results are not unlike those shown in Figs. 3 and 11 for directions parallel to the fibres of the corresponding unidirectional bars. The negative expansion becomes particularly marked at the higher temperatures as a consequence of the increase in the acute inter-ply angle caused by the shear coupling between the plies, and the differences between the thermal expansion coefficients of these specimens and that of pyrolytic graphite in directions perpendicular to the *c*-crystallographic axis, as well as the sense of the variations with temperature, become greater than ever.

5.1.8. Specimens 9 (HTS fibres) and 16 (HMS fibres)

Expansion coefficients corresponding to the directions bisecting the obtuse inter-ply angles of bars 4 and 7 are displayed in Figs. 10 and 17. As is to be expected from the observations recorded so far, the temperature dependence of these results resembles those observed in directions perpendicular to the fibres in the unidirectional bars. The results from specimens 9 and 16 are numerically lower than those for specimens 3 and 11, however. Taken with the results for specimens 8 and 15, these comparisons imply relatively high thermal expansions in directions perpendicular to the planes of the laminates constituting bars 4 and 7. Just as the similarity of the results for specimens 3 and 11 was taken as an indication of the dominant role of the resin in determining the expansion

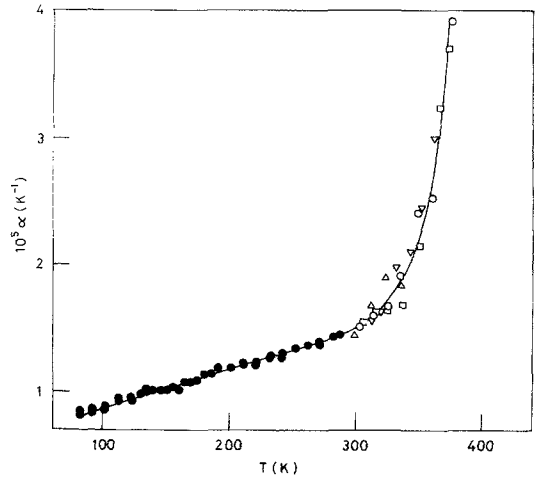

Figure 17 The linear thermal expansion coefficient α of specimens 16: • low temperature runs; ○ 1st, □ 2nd, △ 3rd and ▽ 4th high temperature runs.

characteristics in directions perpendicular to the fibres of unidirectional systems, so the similarity of the results for specimens 9 and 16 indicates the relative importance of the resin over the fibres in determining the expansion in a direction bisecting the obtuse angle of angle-ply laminates.

5.1.9. Specimens 7 (HTS fibres) and 14 (HMS fibres)

One of the more striking features of the results for directions perpendicular to the planes of the two 90° cross-plied laminates displayed in Figs. 8 and 15 is their similarity, which indicates the dominating influence of the resin in determining the thermal expansion characteristics in this direction. The out-of-plane results for the two specimens are higher than the in-plane results by an order of magnitude.

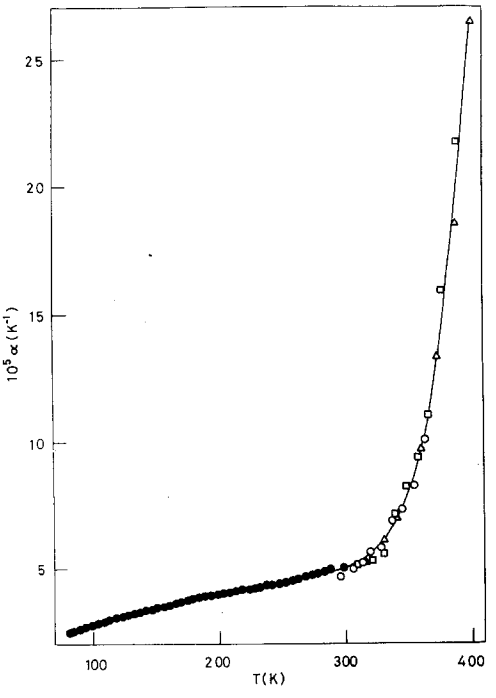

Figure 18 The linear thermal expansion coefficient α of specimens 17: • low temperature runs; ○ 1st, □ 2nd and △ 3rd high temperature runs.

5.1.10. Specimens 17 (HMS fibres)

Corresponding to specimens 7 and 14, attempts were made to prepare specimens having axes perpendidular to the planes of the angle plied bars 4 and 7. Because of the presence of interlaminar cracks in bar 4 which caused delamination problems, this was only possible in the case of bar 7. The results for specimens 17, displayed in Fig. 18, closely resemble those for specimens 7 and 14, and similar remarks apply.

5.2. Analysis of data

In endeavouring to identify a self-consistent scheme which provides a satisfactory account of the present results, the lack of elasticity data at temperatures other than ambient has restricted calculations to this one temperature. For simplicity a standard fibre volume fraction of 50% has been assumed throughout and the angle-ply laminates have been taken to be symmetrically balanced. Subsididiary investigations have indicated that these approximations do not mask the extent to which the practical results conform with expectations based upon the models examined.

5.2.1. The unidirectional case

To attempt to calculate the linear thermal expansion coefficients of the laminates it was necessary to know the elastic moduli of the constituents. In the absence of measurements of some of the values required, recourse was made to theoretical models which provided expressions for the elastic constants of unidirectional composites in terms of the corresponding properties of their constituents.

Smith [15] measured the elastic constants of a series of carbon and graphite fibre-reinforced plastics, one of which consisted of resin ERLA 4617/mPDA containing 64% by volume of Courtaulds HTS carbon fibres. He also measured the elastic constants of this resin separately. Employing the Halpin–Tsai equations [16] and also equations developed by Behrens [17, 18], he calculated the

TABLE III The elastic constants and linear thermal expansion coefficients of the carbon fibres and resin employed in the analysis

	Elastic constants						Linear thermal expansion coefficients		
	$E_{\parallel}$ (GN m^{-2})	$E_{\perp}$ (GN m^{-2})	$G_{\parallel\perp}$ (GN m^{-2})	$G_{\perp\perp}$ (GN m^{-2})	$\nu_{\parallel\perp}$	$\nu_{\perp\parallel}$	$\nu_{\perp\perp}$	$\alpha_{\parallel}$ (× 10^{6} K^{-1})	$\alpha_{\perp}$ (× 10^{6} K^{-1})
HTS fibre	262	13	20	4.6	0.25	0.013	0.40	−1.20	27.3
HMS fibre	411	6.6	20	2.2	0.35	0.006	0.49	−1.20	27.3
Resin	6.9	6.9	2.6	2.6	0.33	0.33	0.33	44.5	44.5

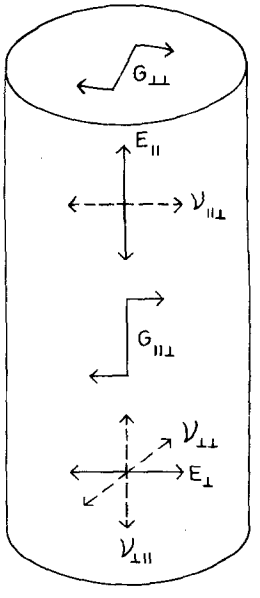

Figure 19 The notation employed in defining the Young's moduli $E_{\parallel}$, $E_{\perp}$, shear moduli $G_{\parallel\perp}$, $G_{\perp\perp}$ and Poisson's ratios $\nu_{\parallel\perp}$, $\nu_{\perp\parallel}$, $\nu_{\perp\perp}$.

elastic constants of the various fibres covered in his investigation. The elastic constants of those of his carbon fibres which resembled most closely those employed in the present investigation have been used to estimate the Young's moduli, shear moduli and Poisson's ratios summarised in Table III. The notation employed in this table follows the form appropriate to transversely isotropic solids illustrated in Fig. 19. The measured results available for the longitudinal Young's moduli, $E_{\parallel}^{f}$, of the HTS and HMS fibres employed in the present investigation were 262 GN m^{-2} and 411 GN m^{-2} respectively. Corresponding values for the transverse direction, $E_{\perp}^{f}$, were obtained by interpolation or extrapolation in graphs of $E_{\parallel}^{f}$ versus $E_{\perp}^{f}$, based upon Smith's results; values of $\nu_{\parallel\perp}^{f}$, $\nu_{\perp\parallel}^{f}$ and $\nu_{\perp\perp}^{f}$ were obtained in a similar manner. The shear modulus $G_{\parallel\perp}^{f}$, was found to be essentially independent of $E_{\parallel}^{f}$ for HMS fibre, while the scatter among the $G_{\parallel\perp}^{f}$ versus $E_{\parallel}^{f}$ results for the HTS fibre led to the adoption of a common value for the two types of fibre. Values of $G_{\perp\perp}^{f}$ were calculated from the equation

$$G_{\perp\perp}^{f} = \frac{E_{\perp}^{f}}{2(1+\nu_{\perp\perp}^{f})}$$

and are included in Table III along with Smith's directly measured results for the elastic moduli of the resin. The longitudinal elastic moduli of specimens 2 and 10 were calculated from the Halpin–Tsai equations. In the case of transversely isotropic fibres these take the mixture-equation forms

$$E_{11}^{c} = E_{\parallel}^{f}V_{f} + E_{m}V_{m} \quad (1)$$

and

$$\nu_{12}^{c} = \nu_{\parallel\perp}^{f}V_{f} + \nu_{m}V_{m} \quad (2)$$

[4] where the subscripts and superscripts m, f and c refer to the matrix, fibre and composite respectively, E_{11}^{c} and ν_{12}^{c} are the longitudinal elastic modulus and Poisson's ratio of the composite, E_{m}, ν_{m} are the Young's modulus and Poisson's ratio of the matrix and V_{f}, V_{m} are the volume fractions of fibre and matrix. The transverse and shear moduli E_{22}^{c} and G_{12}^{c} of these specimens were calculated from the third Halpin–Tsai equation

$$\frac{p_{c}}{p_{m}} = \frac{(1+ZBV_{f})}{(1-BV_{f})} \quad (3)$$

in which $B = (p_{f}/p_{m} - 1)/(p_{f}/p_{m} + Z)$; p_{c} represents E_{22}^{c} or G_{12}^{c}, p_{f} and p_{m} are the appropriate fibre and matrix moduli and Z is a reinforcement factor. From best fits to the results of Adams and Doner [19, 20], Z has been taken as 1.7 in the tensile case and as $[1 + 40(V_{f})^{10}]$ in the case of shear [21]. The results of these calculations for the two specimens are collected in Table IV.

TABLE IV The calculated elastic constants of bars 2 and 5

	E_{11}^{c} (GN m^{-2})	E_{22}^{c} (GN m^{-2})	G_{12}^{c} (GN m^{-2})	ν_{12}^{c}
Bar 2	135	9.56	5.89	0.29
Bar 5	209	6.74	5.89	0.34

For the fibre linear thermal expansion coefficients $\alpha_{\parallel}^{f}$ and $\alpha_{\perp}^{f}$ corresponding to directions parallel and perpendicular to the fibre axis respectively, values corresponding to the a- and c-crystallographic axis directions of pyrolytic graphite [8, 9] were taken. These are included in Table III, together with the measured value for the resin [1].

A variety of theoretical models [22–25] accord with one another, directly or in adapted form, in predicting

$$\alpha_{11}^{c} = \frac{E_{m}\alpha_{m}V_{m} + E_{\parallel}^{f}\alpha_{\parallel}^{f}V_{f}}{E_{m}V_{m} + E_{\parallel}^{f}V_{f}} \quad (4)$$

for the linear thermal expansion coefficient of a uniaxial composite corresponding to those investigated here, in a direction parallel to the fibres, provided that ν_{m} and $\nu_{\parallel\perp}^{f}$ are closely similar. In this equation α_{m} is the linear thermal expansion co-

efficient of the resin and the other terms correspond to the definitions given earlier. Limiting the discussion to the model of Chamberlain [23], who dealt specifically with the case of carbon fibres, the linear thermal expansion coefficient in a direction perpendicular to the fibre axis of a unidirectional composite containing transversely isotropic fibres is given by

$$\alpha_{22}^{c} = \alpha_m + \frac{2(\alpha_{\perp}^{f} - \alpha_m) V_f}{\nu_m(F - 1 + V_m) + (F + V_f) + (E_m/E_{\parallel}^{f})(1 - \nu_{\parallel\perp}^{f})(F - 1 + V_m)} \quad (5)$$

where $F = 0.9069$ for a hexagonal disposition of the fibres and 0.7854 for a square disposition. The results of calculations based upon Equations 4 and 5 are compared with experimental values in Table V. One striking feature of these results is the difference in sensitivity of α_{11}^{c} and α_{22}^{c} to fibre type, corresponding values of α_{11}^{c} differing by a factor of approximately 10 while any differences between corresponding values of α_{22}^{c} were below the limits of detection. These features are compatible with the improved alignment of the α–α planes of the crystallites with the fibre axis in the case of the HMS fibre, small fractional changes in the contribution from c-axis expansion having a much greater influence than equal fractional changes in the contribution from the α–α planes. Figs. 3 and 11 reveal the increase in proportional scatter when the linear thermal expansion coefficient is close to zero. Also, a detailed examination of Equation 4 reveals that small percentage changes in the values taken for $E_{\parallel}^{f}$ produce large percentage changes in the calculated values of α_{11}^{c}. For these two reasons undue significance should not be attached to the numerical differences between the experimental and calculated values of α_{11}^{c}. Examination of the scatter contained by the experimental results displayed in Figs. 4 and 12 and an appraisal of the assumptions made earlier reveal that agreement between the experimental values of α_{22}^{c} and the values calculated from the equations of Chamberlain [23] is remarkably good.

The experimental values of α_{11}^{c} and α_{22}^{c} were applied to calculate the linear thermal expansion coefficient α_{θ}^{c} of unidirectional composites in a direction making an angle θ with the fibre direction, from the equation

$$\alpha_{\theta}^{c} = \alpha_{11}^{c} \cos^2\theta + \alpha_{22}^{c} \sin^2\theta. \quad (6)$$

The results of these calculations are displayed in Figs. 20 and 21. After observing the degree of

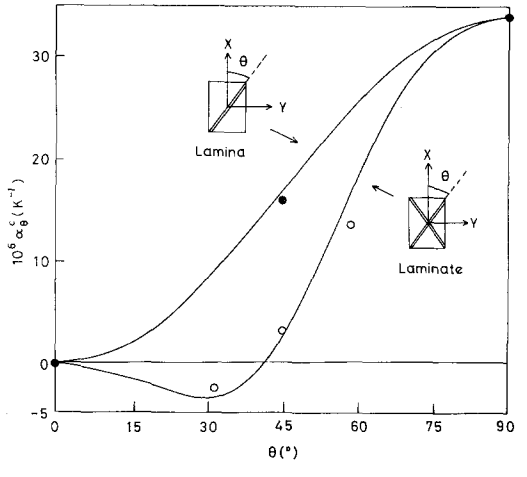

Figure 20 The in-plane linear thermal expansion coefficient α_{θ}^{c} of a unidirectional lamina and a bidirectional laminate of resin ERLA 4617/mPDA reinforced with HTS fibre in directions θ defined in the figure, in which X and Y define the principal axes of the specimens. The lines were calculated as described in the text; the filled circles are experimental results obtained using specimens 2, 3 and 4, the open circles are experimental results obtained using specimens 6, 8 and 9.

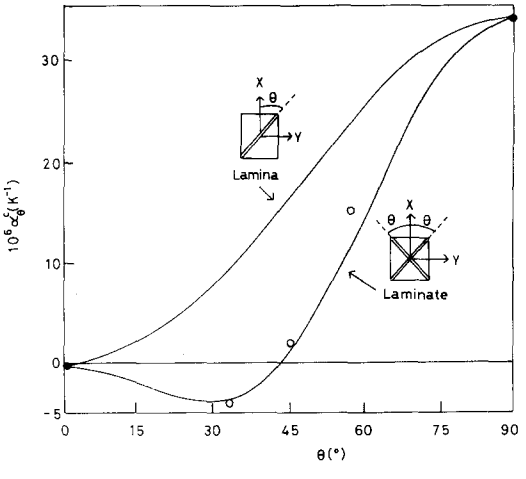

Figure 21 The in-plane linear thermal expansion coefficient α_{θ}^{c} of a unidirectional lamina and a bidirectional laminate of resin ERLA 4617/mPDA reinforced with HMS fibre in directions θ defined in the figure, in which X and Y define the principal axes of the specimens. The lines were calculated as described in the text; the filled circles are experimental results obtained using specimens 10 and 11, the open circles are experimental results obtained using specimens 13, 15 and 16.

TABLE V Measured and calculated linear thermal expansion coefficients of bars 2 and 5

	Bar 2		Bar 5	
	α_{11}^c ($\times 10^6 K^{-1}$)	α_{22}^c ($\times 10^6 K^{-1}$)	α_{11}^c ($\times 10^6 K^{-1}$)	α_{22}^c ($\times 10^6 K^{-1}$)
Experimental	−0.06	33.9	−0.50	33.9
Chamberlain [23] (square array)	−0.03	32.1	−0.44	32.1
Chamberlain [23] (hexagonal array)	−0.03	33.4	−0.44	33.4

accord between the measured and calculated results for specimens 4 [1], no verification for the corresponding results for HMS fibre displayed in Fig. 21 was considered to be necessary.

5.2.2. The bidirectional case

5.2.2.1. In-plane thermal expansion. The in-plane linear thermal expansion coefficients of the angle-ply laminates were calculated for directions bisecting the angles between the two prinicpal fibre directions, using the theory developed by Halpin and Pagano [14]. The experimental data for α_{11}^c and α_{22}^c were employed in association with the elasticity data derived for the laminae, collected in Table IV. The results of these calculations are displayed graphically in Figs. 20 and 21 together with the smoothed experimental data.

5.2.2.2. Out-of-plane thermal expansion. If the individual plies were stacked free and unconnected, the linear thermal expansion coefficient of a cross-plied laminate in a direction perpendicular to the plane of the laminate would be equal to the value corresponding to the direction perpendicular to the fibres of a unidirectional laminate. In practice, however, the expansion of each ply is modified by shear coupling with the neighbouring plies and the out-of-plane expansion becomes a function of interply angle. The details of this dependence have been calculated by Pagano [26], to whose scheme data from the present investigations have been applied. An averaged value of the experimental results for $\nu_{\perp\parallel}^c$ due to Dean and Turner [27] was assumed in this analysis. The results of these calculations are displayed in Figs. 22 and 23, in which the measured and calculated results are compared. As indicated earlier, the presence of inter-laminar cracks in bar 4, although not sufficiently extensive to cause problems in the in-plane measurements, prevented meaningful measurements upon specimens having axes in the direction perpendicular to the plane, so that an experimental point at $\pm 31\frac{1}{2}^\circ$ for Fig. 22 was not available.

6. Appraisal and summary

In assessing the significance which should be attached to the experimental results and the extent to which they conform with expectations

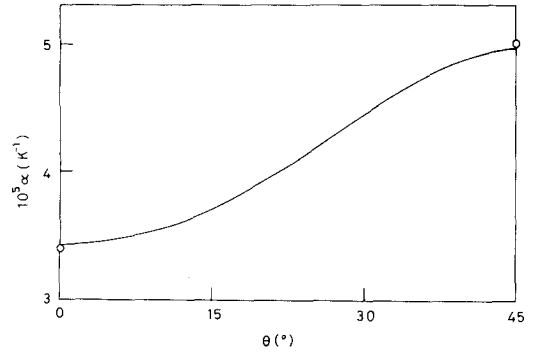

Figure 22 The out-of-plane linear thermal expansion coefficient α of a bidirectional laminate consisting of resin ERLA 4617/mPDA reinforced with HTS fibre, in which θ is half the inter-ply angle. The line was calculated as described in the text; the circles are the experimental results for specimens 3 and 7.

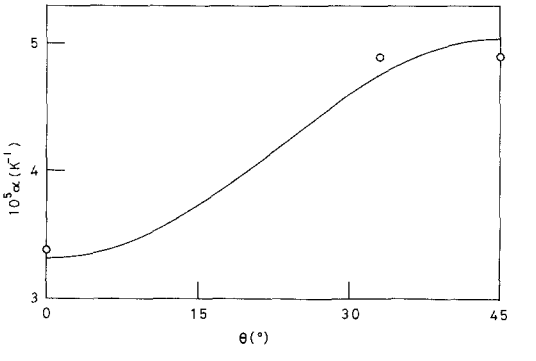

Figure 23 The out-of-plane linear thermal expansion coefficient α of a bidirectional laminate consisting of resin ERLA 4617/mPDA reinforced with HMS fibre, in which θ is half the inter-ply angle. The line was calculated as described in the text; the circles are the experimental results for specimens 11, 17 and 14.

based upon theoretical models, it is desirable to distinguish between physical imperfections associated with the composition of the specimens and mathematical approximations employed in the analyses. Great care was taken in the alignment of the fibres within the specimens during their preparation, but the final alignment was, of necessity, not perfect. Great care was also taken to achieve macroscopically uniform bars. The fact that serious rotations of interference fringe patterns or changes of fringe width were not encountered during the measurements provides testimony to the degree of uniformity of composition attained, although the degree of perfection attainable with a uniformly crystalline material was neither expected nor achieved. A further practical limitation was associated with deviations from uniformity of fibre distribution on the microscopic scale producing effects appropriate to a composite within a composite. In spite of the care taken during specimen preparation, zero void content was seldom achieved and the distribution of the voids actually present was not controlled. The effects of practical limitations such as these can be minimized, but never avoided completely, and their combined effect is very difficult to assess quantitatively. Among the approximations which are more amenable to assessment are the misalignment of specimens during measurement, effects associated with imbalance in laminates containing an odd number of layers of equal thickness and deviations from a constant fibre volume fraction. Calculations indicated that the combined influence of these effects commonly amounted to a few per cent. Additional approximations of a mathematical rather than physical nature were inevitably associated with the assumptions and approximations employed in assessing the elastic constants of the constituents and the linear thermal expansion coefficients of the fibres, though in these cases it is difficult to put limits on the uncertainties involved.

Because of difficulties such as these, overall quantitative assessments of the agreement between experiment and theory would be of questionable value at the present time and a detailed quantitative appraisal must await major extensions of the relevant physical measurements and their interpretations in fundamental terms. In addition to providing data which are available for immediate technological application over a wide range of temperature, however, the investigations have served to provide broad confirmation of current theoretical ideas concerning the directional behaviour of the thermal expansion of unidirectional and bidirectional carbon fibre reinforced plastics.

Acknowledgements

The major part of the work described in this paper was performed under contract to the Ministry of Defence (Procurement Executive), to whom the authors are grateful for financial support received by three of them (M.J.O., J.P.S., and B.A.M.).

References

1. O. PIRGON, G. H. WOSTENHOLM and B. YATES, *J. Phys. D: Appl. Phys.* **6** (1973) 309.
2. B. W. JAMES and B. YATES, *Cryogenics* **5** (1965) 68.
3. A. F. POJUR and B. YATES, *J. Phys. E: Sci. Instrum.* **6** (1973) 63.
4. M. J. OVERY, Ph.D. Thesis, University of Salford, UK (1975).
5. R. K. KIRBY and T. A. HAHN, Data Sheet for NBS SRM 739 dated 12 May 1971, Washington DC, USA.
6. A. A. FAHMY and A. N. RAGAI, *J. Appl. Phys.* **41** (1970) 5112.
7. A. A. FAHMY and A. N. RAGAI-ELLOZY, *J. Comp. Mats.* **8** (1974) 90.
8. A. C. BAILEY and B. YATES, *J. Appl. Phys.* **41** (1970) 5088.
9. B. T. KELLY, B. YATES and O. PIRGON, "The anisotropic thermal expansion of graphite at elevated temperatures", paper 46 in "Proceedings of the Fourth SCI Conference on Industrial Carbons and Graphite", London (1974) to be published.
10. D. J. JOHNSON and C. N. TYSON, *J. Phys. D: Appl. Phys.* **2** (1969) 787.
11. A. FORDEUX, C. HERINCKX, R. PERRET and W. RULAND, *Compt. Rend. Acad. Sci. C* **269** (1969) 1597.
12. B. L. BUTLER and R. J. DIEFENDORF, 9th Biennial Carbon Conference, Summary of Papers, Paper SS25 (1969).
13. R. PERRET and W. RULAND, *J. Appl. Cryst.* **3** (1970) 525.
14. J. C. HALPIN and N. J. PAGANO, AFML-TR-68-395 (1969).
15. R. E. SMITH, *J. Appl. Phys.* **43** (1972) 2555.
16. J. E. ASHTON, J. C. HALPIN and P. H. PETIT, "Primer on Composite Materials: Analysis" (Technomic, Stamford, Conn, 1969) p. 77.
17. E. BEHRENS, *J. Accoust. Soc. Amer.* **45** (1969) 102.
18. Idem, ibid **45** (1969) 1567.
19. D. F. ADAMS and D. R. DONER, *J. Comp. Mats.* **1** (1967) 4.
20. *Idem, ibid* **1** (1967) 152.

21. R. L. HEWITT and M. C. DE MALHERBE, *ibid* 4 (1970) 280.
22. P. S. TURNER, *J. Res. Nat. Bur. Stand.* 37 (1946) 239.
23. N. J. CHAMBERLAIN, BAC Rep. No. SON (P) 33 (1968).
24. R. A. SCHAPERY, *J. Comp. Mats.* 2 (1968) 380.
25. W. SCHNEIDER, *Kunststoffe* 61 (1971) 23.
26. N. J. PAGANO, *J. Comp. Mats.* 8 (1974) 310.
27. G. D. DEAN and P. TURNER, *Composites* 4 (1973) 174.

Received 27 July and accepted 31 August 1976.